Eur. Phys. J. B **16**, 411–422 (2000)

The European Physical Journal B

EDP Sciences
© Società Italiana di Fisica
Springer-Verlag 2000

Magneto-optical Kerr effect in bilayer structures

N. Richard[a]

Abteilung Experimentelle Physik, Albert-Einstein Allee 11, 89069 Universität Ulm, Germany

Received 26 January 2000

Abstract. This paper describes the magneto-optical effects and the reflectivity behaviors of bilayers based on magnetic and isotropic (MgF_2)/anisotropic (TiO_2) layers under the condition of total internal reflection. In the framework of Green's dyadic technique, we show accurately the optical properties of anisotropic layers deposited on a substrate. We present numerical simulations which account for the variation of angle of incidence at the HeNe laser wavelength. The Kerr rotation is found to increase significantly around the optical modes in total reflection. We also discuss the importance of anisotropic effects due to the crystallization of the dielectric material (TiO_2) which occur in the reflectivity and Kerr rotation spectra.

PACS. 78.20.Ci Optical constants (including refractive index, complex dielectric constant, absorption, reflection and transmission coefficients, emissivity) – 78.20.Ls Magnetooptical effects – 78.66.-w Optical properties of specific thin films, surfaces, and low-dimensional structures

1 Introduction

The magneto-optical Kerr effect has become an important magnetic characterization technique in the topic of magnetic ultrathin films and multilayers [1–3] and is also used in optical reading devices [4–8]. Recent works have studied the Kerr effect of multilayers made of magnetic materials by illuminating through a transparent substrate at fixed wavelength as a function of the angle of incidence [9], this brings to the fore the role of surface plasmon [10,11] in the magneto-optical signal.

In this paper, we analyse accurately other kinds of resonances occurring in the reflectivity and in the magneto-optical Kerr rotation module as a function of the angle of incidence for a multilayer system, and especially the interferences in dielectric films [12]. In this context, we study theoretically phenomena relative to bilayers composed of a magneto-optical film and an isotropic/anisotropic dielectric layer deposited on a glass substrate for the HeNe laser wavelength ($\lambda = 633$ nm). We underline the role of resonance phenomena in the bilayer structure. The numerical method used for these calculations is based on the Green's dyadic technique [13,14] which can account for any kind of linear anisotropy. The films are illuminated through the substrate beyond the critical angle for total internal reflection. The two polarization modes TE and TM are considered for the incident electric field associated to the laser beam. In the TE mode, the incident electric field is perpendicular to the plane of incidence (the so-called s-polarization) whereas this field is parallel to it in the TM mode (the p-polarization).

[a] e-mail: Nicolas.Richard@physik.uni-ulm.de

2 Optical properties of an anisotropic multilayer system

2.1 Scattering theory

Our theoretical analysis of the propagation of electromagnetic fields through an arbitrary anisotropic multilayered structure is based on scattering theory. In this theory, one describes the scattering of waves relative to a reference system. In the context of multilayers, it is convenient to choose such a system as the single surface geometry made of two semi-infinite isotropic media [15]. Let $\varepsilon_1(z,\omega)$ be the frequency (ω) dependent dielectric function profile of this surface system.

Assuming that the fields have an harmonic time dependence $e^{-i\,\omega\, t}$ in Maxwell's equations, the vectorial wave equation satisfied by the electric field is (c is the speed of light in vacuum):

$$-\nabla\times\nabla\times\mathbf{E}(\mathbf{r})+\frac{\omega^2}{c^2}\,\varepsilon_1(z,\omega)\,\mathbf{E}(\mathbf{r})=\mathsf{V}(z,\omega)\,\mathbf{E}(\mathbf{r}). \quad (1)$$

For $z>0$, $\varepsilon_1(z,\omega)$ corresponds to the dielectric function of the external medium:

$$\varepsilon_1(z,\omega)=\varepsilon_{\mathrm{a}}(\omega),$$

while for $z<0$, $\varepsilon_1(z,\omega)$ is given by the dielectric function of the substrate:

$$\varepsilon_1(z,\omega)=\varepsilon_{\mathrm{sub}}(\omega).$$

The perturbation dyadic $\mathsf{V}(z,\omega)$ is defined by (Fig. 1a):

$$\mathsf{V}(z,\omega)=\frac{\omega^2}{c^2}\,(1\,\varepsilon_a(\omega)-\varepsilon(z,\omega))\quad(z>0), \quad (2)$$

$$\mathsf{V}(z,\omega)=0\qquad(z<0), \quad (3)$$

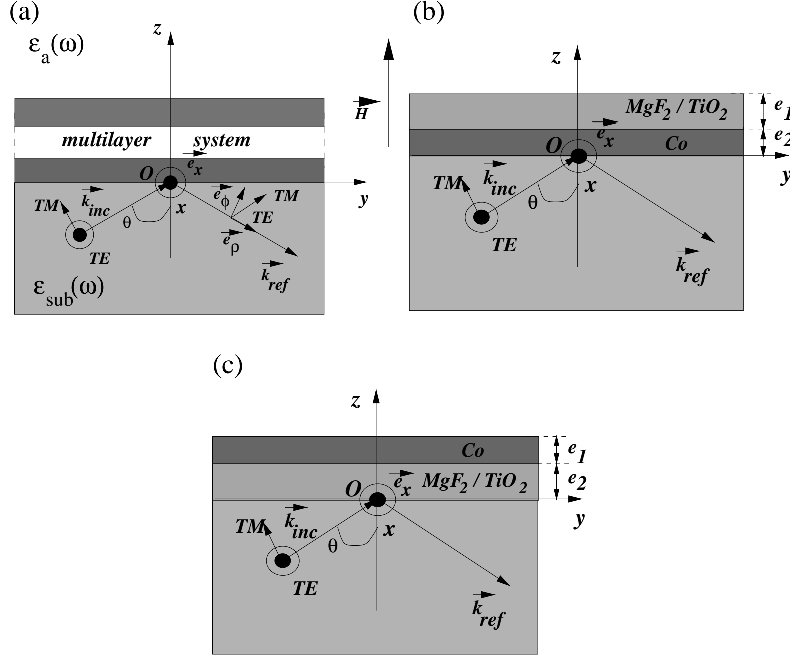

Fig. 1. (a) Geometry of the system. We define $\mathbf{r} = \mathbf{r}_\| + z\ \mathbf{e}_z$, $\mathbf{r}' = \mathbf{r}'_\| + z'\ \mathbf{e}_z$ and $\mathbf{k} = \mathbf{k}_\| + k_z\ \mathbf{e}_z$, the cylindrical coordinates ($\mathbf{e}_x$, $\mathbf{e}_\rho$, $\mathbf{e}_\phi$) are used to define the Kerr effect. The radial coordinate $\mathbf{e}_\rho$ is aligned along the reflected wavevector. (b) Configuration of total reflection in the case of a bilayer Co/MgF_2 with $e_1 = 100$ nm, 200 nm and 400 nm, $e_2 = 10$ nm and in the case of a bilayer Co/TiO_2 with $e_1 = 450$ nm and $e_2 = 10$ nm. (c) Configuration of total reflection in the case of a bilayer MgF_2/Co with $e_1 = 100$ nm and $e_2 = 2000$ nm and in the case of a bilayer TiO_2/Co with $e_1 = 100$ nm and $e_2 = 1100$ nm.

$\varepsilon(z,\omega)$ is the dielectric tensor of the multilayered structure which is located in the upper z plane ($z' > 0$). The structure of this tensor is not limited to magneto-optical materials. It can account for any kind of linear anisotropy.

The solution of the scattering problem is given by the Lippmann-Schwinger equation:

$$\mathbf{E}(\mathbf{r}) = \mathbf{E}^0(\mathbf{r}) + \mathbf{E}^{\mathrm{s}}(\mathbf{r}) \tag{4}$$

where $\mathbf{E}^0(\mathbf{r})$ and $\mathbf{E}^{\mathrm{s}}(\mathbf{r})$ are the incident and the scattered field.

The scattered field is given by (A is the domain where $\mathsf{V}(z',\omega) \neq 0$):

$$\mathbf{E}^{\mathrm{s}}(\mathbf{r}) = \int_A \mathrm{d}\mathbf{r}'\ \mathsf{G}(\mathbf{r},\mathbf{r}';\omega)\ \mathsf{V}(z',\omega)\ \mathbf{E}(\mathbf{r}'). \tag{5}$$

In this last equation, $\mathsf{G}(\mathbf{r},\mathbf{r}';\omega)$ is the Green's dyadic defined by ($\delta(\mathbf{r}-\mathbf{r}')$ is the Dirac delta function):

$$-\nabla\times\nabla\times\mathsf{G}(\mathbf{r},\mathbf{r}';\omega) + \frac{\omega^2}{c^2}\ \varepsilon_1(z,\omega)\ \mathsf{G}(\mathbf{r},\mathbf{r}';\omega) = 1\ \delta(\mathbf{r}-\mathbf{r}'). \tag{6}$$

The planar symmetry of multilayered structures allows the introduction of following Fourier expansions for the fields and the propagator involved in (4, 5) and (6):

$$\mathbf{E}(\mathbf{r}) = \frac{1}{4\,\pi^2}\int \mathrm{d}\mathbf{k}_\|\ \mathbf{F}(z;\mathbf{k}_\|)\ \mathrm{e}^{\mathrm{i}\ \mathbf{k}_\|\cdot\mathbf{r}_\|} \tag{7}$$

$$\mathbf{E}_0(\mathbf{r}) = \frac{1}{4\,\pi^2}\int \mathrm{d}\mathbf{k}_\|\ \mathbf{F}_0(z;\mathbf{k}_\|)\ \mathrm{e}^{\mathrm{i}\ \mathbf{k}_\|\cdot\mathbf{r}_\|} \tag{8}$$

$$\mathsf{G}(\mathbf{r},\mathbf{r}';\omega) = \frac{1}{4\,\pi^2}\int \mathrm{d}\mathbf{k}_\|\ \mathrm{e}^{\mathrm{i}\ \mathbf{k}_\|\cdot(\mathbf{r}_\|-\mathbf{r}_\|{}')}\ \mathsf{g}(z,\mathrm{z}';\mathbf{k}_\|). \tag{9}$$

The introduction of the Fourier transforms (7–9) in equation (4) leads to a one-dimensional vector Lippmann-Schwinger equation:

$$\mathbf{F}(z;\mathbf{k}_\|) = \mathbf{F}_0(z;\mathbf{k}_\|) + \int_A \mathrm{d}z'\ \mathsf{g}(z,z';\mathbf{k}_\|)\ \mathsf{V}(z',\omega)\ \mathbf{F}(z';\mathbf{k}_\|). \tag{10}$$

The numerical analysis is based on the discretization of this last Lippmann-Schwinger equation [14].

The source coordinate z' being positive, for $z > 0$, the dyadic $\mathsf{g}(z,z';\mathbf{k}_\|)$ is the sum of the dyadic Green tensor associated to the external medium $\mathsf{g}_0(z,z';\mathbf{k}_\|)$ and the surface response $\mathsf{g}_{\mathrm{s}}(z,z';\mathbf{k}_\|)$:

$$\mathsf{g}(z,z';\mathbf{k}_\|) = \mathsf{g}_0(z,z';\mathbf{k}_\|) + \mathsf{g}_{\mathrm{s}}(z,z';\mathbf{k}_\|). \tag{11}$$

For $z < 0$, the dyadic is reduced to one term:

$$\mathsf{g}(z,z';\mathbf{k}_\|) = \mathsf{g}'_{\mathrm{s}}(z,z';\mathbf{k}_\|). \tag{12}$$

2.2 The Green's dyadic for a surface system

We detail here the analytical structure of $\mathsf{g}(z,z';\mathbf{k}_\|)$. We first precise the two possible values of the wavevector component along $\mathbf{e}_z$ ($k_\|^2 = k_x^2 + k_y^2$):

$$k_{\mathrm{a}} = \sqrt{\frac{\omega^2}{c^2}\ \varepsilon_{\mathrm{a}} - k_\|^2} \tag{13}$$

$$k_{\mathrm{sub}} = \sqrt{\frac{\omega^2}{c^2}\ \varepsilon_{\mathrm{sub}} - k_\|^2}. \tag{14}$$

In the case where $z > 0$ and $z' > 0$, we find for $\mathsf{g}_\mathrm{s}(z, z'; \mathbf{k}_\parallel)$:

$$\mathsf{g}_0(z, z'; \mathbf{k}_\parallel) = \frac{\mathrm{e}^{\mathrm{i}\, k_a\, |z-z'|}}{2\,\mathrm{i}\, k_\mathrm{a}} \left(1 - \frac{c^2}{\omega^2\, \varepsilon_\mathrm{a}}\, \mathsf{Q}\right) + \frac{c^2}{\omega^2\, \varepsilon_\mathrm{a}}\, \mathsf{L}\, \delta(z - z') \tag{15}$$

with

$$\mathsf{Q} = \begin{pmatrix} k_x^2 & k_x\, k_y & \frac{|z-z'|}{z-z'}\, k_x\, k_\mathrm{a} \\ k_x\, k_y & k_y^2 & \frac{|z-z'|}{z-z'}\, k_y\, k_\mathrm{a} \\ \frac{|z-z'|}{z-z'}\, k_x\, k_\mathrm{a} & \frac{|z-z'|}{z-z'}\, k_y\, k_\mathrm{a} & k_\mathrm{a}^2 \end{pmatrix}. \tag{16}$$

The tensor

$$\mathsf{L} = \begin{pmatrix} 0\,0\,0 \\ 0\,0\,0 \\ 0\,0\,1 \end{pmatrix} \tag{17}$$

accounts for the depolarization of a discretized cell which has the shape of a very thin film [16].

The dyadic $\mathsf{g}_\mathrm{s}(z, z'; \mathbf{k}_\parallel)$ describing the surface response when $z > 0$ is:

$$\mathsf{g}_\mathrm{s}(z, z'; \mathbf{k}_\parallel) = \begin{pmatrix} \frac{k_x^2}{k_\parallel^2} D_{xx} + \frac{k_y^2}{k_\parallel^2} D_{yy} & \frac{k_x k_y}{k_\parallel^2}(D_{xx} - D_{yy}) & \frac{k_x}{k_\parallel} D_{xz} \\ \frac{k_x k_y}{k_\parallel^2}(D_{xx} - D_{yy}) & \frac{k_y^2}{k_\parallel^2} D_{xx} + \frac{k_x^2}{k_\parallel^2} D_{yy} & \frac{k_y}{k_\parallel} D_{xz} \\ \frac{k_x}{k_\parallel} D_{zx} & \frac{k_y}{k_\parallel} D_{zx} & D_{zz} \end{pmatrix} \tag{18}$$

where

$$D_{xx} = -\frac{c^2}{\omega^2\, \varepsilon_\mathrm{a}}\, k_\mathrm{a}^2\, \frac{k_\mathrm{a}\, \varepsilon_\mathrm{sub} - k_\mathrm{sub}\, \varepsilon_\mathrm{a}}{k_\mathrm{a}\, \varepsilon_\mathrm{sub} + k_\mathrm{sub}\, \varepsilon_\mathrm{a}}\, \frac{\mathrm{e}^{\mathrm{i}\, k_\mathrm{a}\, (z+z')}}{2\,\mathrm{i}\, k_\mathrm{a}} \tag{19}$$

$$D_{yy} = \frac{k_\mathrm{a} - k_\mathrm{sub}}{k_\mathrm{a} + k_\mathrm{sub}}\, \frac{\mathrm{e}^{\mathrm{i}\, k_\mathrm{a}\, (z+z')}}{2\,\mathrm{i}\, k_\mathrm{a}} \tag{20}$$

$$D_{zx} = \frac{c^2}{\omega^2\, \varepsilon_\mathrm{a}\, k_\mathrm{a}}\, k_\parallel\, \frac{k_\mathrm{a}\, \varepsilon_\mathrm{sub} - k_\mathrm{sub}\, \varepsilon_\mathrm{a}}{k_\mathrm{a}\, \varepsilon_\mathrm{sub} + k_\mathrm{sub}\, \varepsilon_\mathrm{a}}\, \frac{\mathrm{e}^{\mathrm{i}\, k_\mathrm{a}\, (z+z')}}{2\,\mathrm{i}\, k_\mathrm{a}} \tag{21}$$

$$D_{xz} = -\frac{c^2}{\omega^2\, \varepsilon_\mathrm{a}}\, k_\mathrm{a}\, k_\parallel\, \frac{k_\mathrm{a}\, \varepsilon_\mathrm{sub} - k_\mathrm{sub}\, \varepsilon_\mathrm{a}}{k_\mathrm{a}\, \varepsilon_\mathrm{sub} + k_\mathrm{sub}\, \varepsilon_\mathrm{a}}\, \frac{\mathrm{e}^{\mathrm{i}\, k_\mathrm{a}\, (z+z')}}{2\,\mathrm{i}\, k_\mathrm{a}} \tag{22}$$

$$D_{zz} = \frac{c^2}{\omega^2\, \varepsilon_\mathrm{a}}\, k_\parallel^2\, \frac{k_\mathrm{a}\, \varepsilon_\mathrm{sub} - k_\mathrm{sub}\, \varepsilon_\mathrm{a}}{k_\mathrm{a}\, \varepsilon_\mathrm{sub} + k_\mathrm{sub}\, \varepsilon_\mathrm{a}}\, \frac{\mathrm{e}^{\mathrm{i}\, k_\mathrm{a}\, (z+z')}}{2\,\mathrm{i}\, k_\mathrm{a}}. \tag{23}$$

For $z < 0$ and $z' > 0$, the dyadic $\mathsf{g}(z, z'; \mathbf{k}_\parallel)$ is only due to the response of the surface $\mathsf{g}'_\mathrm{s}(z, z'; \mathbf{k}_\parallel)$ which has the same structure as equation (18) but with the following coefficients:

$$D_{xx} = -\mathrm{i}\, \frac{c^2}{\omega^2}\, \frac{k_\mathrm{a}\, k_\mathrm{sub}}{k_\mathrm{a}\, \varepsilon_\mathrm{sub} + k_\mathrm{sub}\, \varepsilon_\mathrm{a}}\, \mathrm{e}^{\mathrm{i}\, k_\mathrm{a}\, z' - \mathrm{i}\, k_\mathrm{sub}\, z} \tag{24}$$

$$D_{yy} = -\frac{\mathrm{i}}{k_\mathrm{a} + k_\mathrm{sub}}\, \mathrm{e}^{\mathrm{i}\, k_\mathrm{a}\, z' - \mathrm{i}\, k_\mathrm{sub}\, z} \tag{25}$$

$$D_{zx} = -\mathrm{i}\, \frac{c^2}{\omega^2}\, \frac{k_\mathrm{a}\, k_\parallel}{k_\mathrm{a}\, \varepsilon_\mathrm{sub} + k_\mathrm{sub}\, \varepsilon_\mathrm{a}}\, \mathrm{e}^{\mathrm{i}\, k_\mathrm{a}\, z' - \mathrm{i}\, k_\mathrm{sub}\, z} \tag{26}$$

$$D_{xz} = -\mathrm{i}\, \frac{c^2}{\omega^2}\, \frac{k_\mathrm{sub}\, k_\parallel}{k_\mathrm{a}\, \varepsilon_\mathrm{sub} + k_\mathrm{sub}\, \varepsilon_\mathrm{a}}\, \mathrm{e}^{\mathrm{i}\, k_\mathrm{a}\, z' - \mathrm{i}\, k_\mathrm{sub}\, z} \tag{27}$$

$$D_{zz} = -\mathrm{i}\, \frac{c^2}{\omega^2}\, \frac{k_\parallel^2}{k_\mathrm{a}\, \varepsilon_\mathrm{sub} + k_\mathrm{sub}\, \varepsilon_\mathrm{a}}\, \mathrm{e}^{\mathrm{i}\, k_\mathrm{a}\, z' - \mathrm{i}\, k_\mathrm{sub}\, z}. \tag{28}$$

2.3 Far-field properties

Considering the reflected electric field in the far field allows some analytical simplifications. In the case of illumination through the substrate, the reflected field reads ($z < 0$):

$$\mathbf{E}_\mathrm{r}(\mathbf{r}) = \frac{1}{4\,\pi^2} \int \mathrm{d}\mathbf{k}_\parallel\, \mathbf{f}_\mathrm{r}(\mathbf{k}_\parallel)\, \mathrm{e}^{\mathrm{i}\, \mathbf{k}_\parallel \cdot \mathbf{r}_\parallel}\, \mathrm{e}^{-\mathrm{i}\, k_\mathrm{sub}\, z} \tag{29}$$

where

$$\mathbf{f}_\mathrm{r}(\mathbf{k}_\parallel) = \int_A \mathrm{d}z'\, \mathsf{g}'_\mathrm{s}(0, z'; \mathbf{k}_\parallel)\, \mathsf{V}(z', \omega)\, \mathbf{F}(z'; \mathbf{k}_\parallel). \tag{30}$$

In the simple case where the incident field has the form of a plane wave, we have of course:

$$\mathbf{F}_0(z; \mathbf{k}_\parallel) = \mathbf{A}\, \mathrm{e}^{\mathrm{i}\, k_\mathrm{sub}\, z}\, \delta(\mathbf{q}_\parallel - \mathbf{k}_\parallel) + \mathbf{A}_1\, \mathrm{e}^{-\mathrm{i}\, k_\mathrm{sub}\, z}\, \delta(\mathbf{q}_\parallel - \mathbf{k}_\parallel) \qquad (z < 0) \tag{31}$$

$$\mathbf{F}_0(z; \mathbf{k}_\parallel) = \mathbf{A}_2\, \mathrm{e}^{\mathrm{i}\, k_\mathrm{a}\, z}\, \delta(\mathbf{q}_\parallel - \mathbf{k}_\parallel) \qquad (z > 0) \tag{32}$$

where we normalize the TE mode according to:

$$\mathbf{A} = \mathbf{e}_x \tag{33}$$

$$\mathbf{A_1} = \frac{k_\mathrm{sub} - k_\mathrm{a}}{k_\mathrm{sub} + k_\mathrm{a}}\, \mathbf{e}_x \tag{34}$$

$$\mathbf{A_2} = \frac{2\, k_\mathrm{sub}}{k_\mathrm{sub} + k_\mathrm{a}}\, \mathbf{e}_x \tag{35}$$

and the TM mode as follows:

$$\mathbf{A} = -\cos\theta\, \mathbf{e}_y + \sin\theta\, \mathbf{e}_z \tag{36}$$

$$\mathbf{A}_1 = \frac{k_\mathrm{sub}\, \varepsilon_\mathrm{a} - k_\mathrm{a}\, \varepsilon_\mathrm{sub}}{k_\mathrm{sub}\, \varepsilon_\mathrm{a} + k_\mathrm{a}\, \varepsilon_\mathrm{sub}} (\cos\theta\, \mathbf{e}_y + \sin\theta\, \mathbf{e}_z) \tag{37}$$

$$\mathbf{A}_2 = \frac{2\, k_\mathrm{sub}\, \sqrt{\varepsilon_\mathrm{a}}\, \sqrt{\varepsilon_\mathrm{sub}}}{k_\mathrm{sub}\, \varepsilon_\mathrm{a} + k_\mathrm{a}\, \varepsilon_\mathrm{sub}} (-\cos\theta_\mathrm{t}\, \mathbf{e}_y + \sin\theta_\mathrm{t}\, \mathbf{e}_z) \tag{38}$$

θ is the angle of reflection, θ_t is the angle of transmission, $\mathbf{q}_\parallel = \sin\theta\, \mathbf{e}_y$ and $q = \frac{\omega^2}{c^2}\, \varepsilon_1(z, \omega)$.

For the reflection, the scattered field (29) is then reduced to ($z < 0$):

$$\mathbf{E}_\mathrm{r}(\mathbf{r}) = \frac{1}{4\,\pi^2}\, [\mathbf{A}_1 + \mathbf{f}_\mathrm{r}(\mathbf{q}_\parallel)]\, \mathrm{e}^{\mathrm{i}\, \mathbf{q}_\parallel \cdot \mathbf{r}_\parallel}\, \mathrm{e}^{-\mathrm{i}\, k_\mathrm{sub}\, z}. \tag{39}$$

The reflectivity outside the multilayer arises then as:

$$R = \frac{\left|\mathbf{A}_1 + \mathbf{f}_\mathrm{r}(\mathbf{q}_\parallel)\right|^2}{|\mathbf{A}|^2}. \tag{40}$$

2.4 Kerr effect

The Kerr effect is described by a rotation of the plane of polarization of the reflected field relative to the incident field. A set of cylindrical coordinates (Fig. 1a) based on the reflected wavevector is introduced by:

$$\begin{aligned} f_{\mathrm{r},\rho}(\mathbf{k}_\parallel) &= f_{\mathrm{r},y}(\mathbf{k}_\parallel)\, \sin\,\theta - f_{\mathrm{r},z}(\mathbf{k}_\parallel)\, \cos\,\theta \\ f_{\mathrm{r},\phi}(\mathbf{k}_\parallel) &= f_{\mathrm{r},y}(\mathbf{k}_\parallel)\, \cos\,\theta + f_{\mathrm{r},z}(\mathbf{k}_\parallel)\, \sin\,\theta \\ f_{\mathrm{r},x}(\mathbf{k}_\parallel) &= f_{\mathrm{r},x}(\mathbf{k}_\parallel). \end{aligned} \tag{41}$$

The Kerr rotations Φ_s' and Φ_p' and the ellipticities Φ_s'' and Φ_p'' correspond to the real and imaginary part of the following ratios:

$$\Phi_s = \frac{f_{r,\phi}(\mathbf{k}_\parallel)}{f_{r,x}(\mathbf{k}_\parallel)} = \Phi_s' + \mathrm{i}\,\Phi_s'' \;\; \text{(TE)} \tag{42}$$

$$\Phi_p = \frac{f_{r,x}(\mathbf{k}_\parallel)}{f_{r,\phi}(\mathbf{k}_\parallel)} = \Phi_p' + \mathrm{i}\,\Phi_p'' \;\; \text{(TM).} \tag{43}$$

In this paper, we use the Co as a generic example of magneto-optical material. The case of the polar magnetization will be considered alone because longitudinal magnetization produces signals which are one order of magnitude weaker. The polar magnetization corresponds to an applied static magnetic field which is perpendicular to the interfaces, thus along the z direction. The polar magnetization gives the following structure of the dielectric tensor for $\lambda = 633$ nm:

$$\varepsilon_{\text{polar}} = \begin{pmatrix} \alpha & \beta & 0 \\ -\beta & \alpha & 0 \\ 0 & 0 & \alpha \end{pmatrix} \tag{44}$$

where the coefficients $\alpha = -12.3 + \mathrm{i}\,18.4$ and $\beta = -0.4 - \mathrm{i}\,0.1$ were found in reference [17,18]. We use MgF_2 and TiO_2 for the dielectric materials. MgF_2 is an isotropic material which dielectric tensor can be written as follows for $\lambda = 633$ nm:

$$\varepsilon_{MgF_2} = \begin{pmatrix} 1.9 & 0 & 0 \\ 0 & 1.9 & 0 \\ 0 & 0 & 1.9 \end{pmatrix}\cdot \tag{45}$$

The rutile (TiO_2) is an anisotropic uniaxial crystal, this is due to its crystalline structure [19]. The deposition of thin rutile films is difficult to realize and the anisotropic behaviour is hard to obtain because its deposition in thin films imposes its amorphous behaviour. Except for this problem, we will show in this study, that anisotropy on thin films can give satisfying results from an optical point of view. We examine how the reflectivity and also the Kerr rotation behave facing the optical anisotropy for this material.

If we align the eigen axis of the rutile crystal along our coordinate system $Oxyz$, the dielectric tensor has the following form:

$$\varepsilon^1_{TiO_2} = \begin{pmatrix} \varepsilon_1 & 0 & 0 \\ 0 & \varepsilon_1 & 0 \\ 0 & 0 & \varepsilon_2 \end{pmatrix} \tag{46}$$

with $\varepsilon_1 = 6.67$ and $\varepsilon_2 = 8.24$ which are the dielectric permittivities related to the ordinary (ε_1) and to the extraordinary (ε_2) index of refraction for the HeNe wavelength ($\lambda = 633$ nm).

We can modify the orientation of the principal axis for the rutile (46) by a circular rotation of 90 degrees along the (Ox) axis in our coordinate system, it can be written as follows:

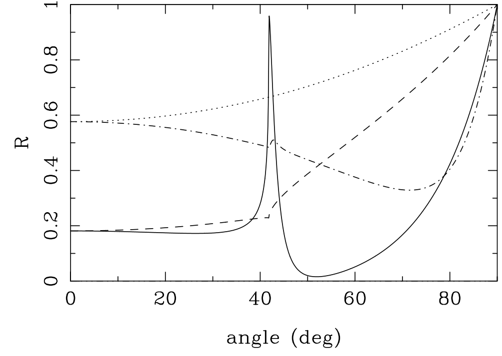

Fig. 2. For $\lambda = 0.633$ μm, reflected energy of a 10 nm (TM mode: solid line, TE mode: dashed line) and a 60 nm (TM: dotted dashed line, TE mode: dotted line) Co film deposited on a glass substrate as a function of the angle of incidence.

$$\varepsilon^2_{TiO_2} = \begin{pmatrix} \varepsilon_1 & 0 & 0 \\ 0 & \varepsilon_2 & 0 \\ 0 & 0 & \varepsilon_1 \end{pmatrix}\cdot \tag{47}$$

On the same way, we can define another orientation:

$$\varepsilon^3_{TiO_2} = \begin{pmatrix} \varepsilon_2 & 0 & 0 \\ 0 & \varepsilon_1 & 0 \\ 0 & 0 & \varepsilon_1 \end{pmatrix}\cdot \tag{48}$$

The three types of orientation for the principal axis of the crystal are materialized in the dielectric tensor by the expressions (46), (47) and (48).

Each one will be studied in order to observe reflectivity and Kerr rotation changes as a function of the angle of incidence by the modification of the diagonal terms which occur in the dielectric tensor of TiO_2.

3 Magnetic/dielectric bilayers

3.1 Co/MgF_2 bilayer

We have chosen to set a 10 nm Co film thickness on a glass substrate in order to limit the absorption. Moreover, this thickness corresponds to a plasmon resonance which appears for an angle close to 51 degrees in the reflectivity curve as a function of the angle of incidence for the TM mode. One must be aware that the natural magnetization state of a 10 nm thick Co film is parallel to the surface. Static fields as high as 2 teslas are needed to pull the magnetization out of plane. Nevertheless, the 10 nm Co film can be replaced by Co $-$ Pt or Co $-$ Au ultrathin multilayers, known to have strong perpendicular magnetic anisotropy, without affecting the results discussed here.

In this curve (Fig. 2), the virtual modes, responsible of Perot-Fabry interferences, show up between the critical angle at 41.8 degrees and 43 degrees as a peak which is more accentuated compared to a noble metal such as gold

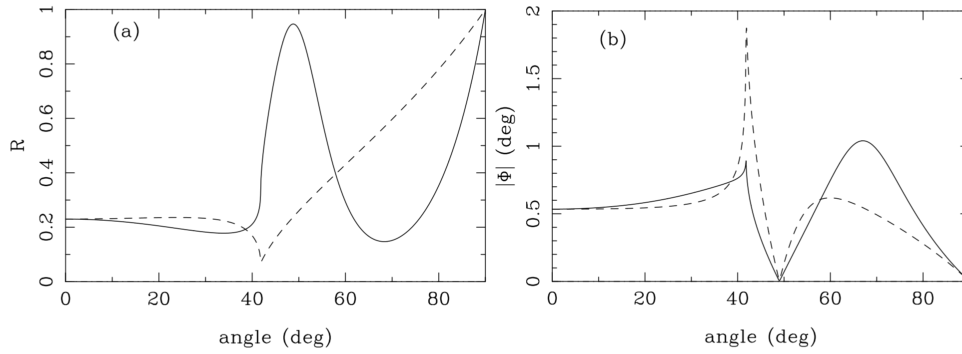

Fig. 3. For $\lambda = 0.633$ μm, (a) reflectivity of a bilayer composed of 10 nm of Co and of 100 nm of MgF_2 deposited on a glass substrate for the two modes: TE (dashed line) and TM (solid line) as a function of the angle of incidence (b) module $|\Phi|$ as a function of the angle of incidence for the two modes: TE (dashed line) and TM (solid line) in the polar magnetization case.

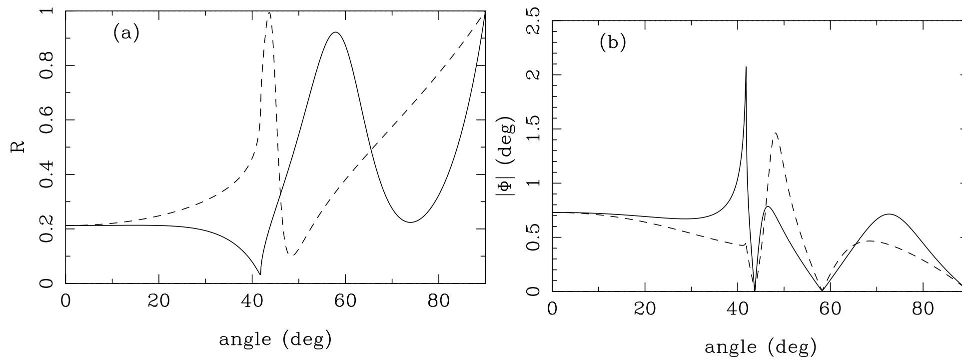

Fig. 4. For $\lambda = 0.633$ μm, (a) reflectivity of a bilayer composed of 10 nm of Co and of 200 nm of MgF_2 deposited on a glass substrate for the two modes: TE (dashed line) and TM (solid line) as a function of the angle of incidence (b) module $|\Phi|$ as a function of the angle of incidence for the two modes: TE (dashed line) and TM (solid line) in the polar magnetization case.

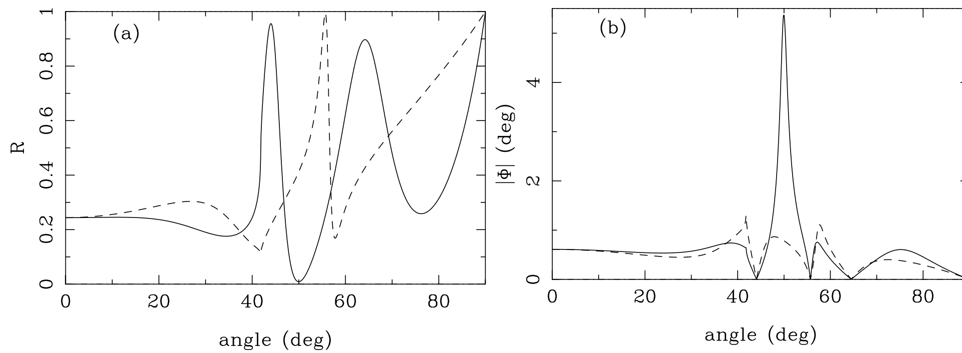

Fig. 5. For $\lambda = 0.633$ μm, (a) reflectivity of a bilayer composed of 10 nm of Co and of 400 nm of MgF_2 deposited on a glass substrate for the two modes: TE (dashed line) and TM (solid line) as a function of the angle of incidence (b) module $|\Phi|$ as a function of the angle of incidence for the two modes: TE (dashed line) and TM (solid line) in the polar magnetization case.

or silver. The reflectivity, in this angular range, shows exponential damped oscillations as a function of the Co film thickness as we have noticed for gold (see Ref. [13]).

The presence of these modes creates reflectivity oscillations as a function of the angle of incidence beyond the critical angle by addition of a dielectric film on the cobalt one. Indeed, we will study a bilayer composed of a 10 nm of Co thin film recovered by a MgF_2 dielectric film for which we vary the film thickness, they are both deposited on a glass substrate (see Fig. 1b). We will take successively 100 nm, 200 nm and 400 nm for the different MgF_2 film thicknesses (the effective wavelength in the MgF_2 is approximatively $\lambda_{\text{eff}}^{\text{MgF}_2} = 458$ nm, these thicknesses correspond to $\lambda_{\text{eff}}^{\text{MgF}_2}/4$, $\lambda_{\text{eff}}^{\text{MgF}_2}/2$ and $\lambda_{\text{eff}}^{\text{MgF}_2}$). The cobalt thickness was chosen so as to let the energy going through the Co layer and consequently, to create interferences in the dielectric film.

In the TM mode, these interferences are materialized by oscillations in the reflectivity curve as a function of the angle of incidence by addition to an increasing MgF_2 film thickness (see Figs. 3a, 4a and 5a). We can notice that the higher is the dielectric film thickness, the higher is the number of oscillations which occur in the reflectivity curve for the TM mode. Thus, it brings to

the fore the effects due to constructive and destructive interferences in the dielectric film.

In the TE mode, when the MgF_2 dielectric film is missing, the reflectivity curve does not show any particular behaviour except its regular increase as a function of the angle of incidence for a 10 nm Co layer deposited on a glass substrate. However, the presence of an increasing MgF_2 film thickness modifies the reflectivity curve and oscillations occur as the TM mode shows. This is due to multiple reflections in the MgF_2 layer (see Figs. 3a, 4a and 5a), the eigen modes of the system induced by multiple reflections in the dielectric layer influenced the oscillation behaviours of the reflectivity curve in the TE mode. At this step, we can conclude that the presence of the dielectric layer deposited on a thin metallic layer involves oscillations in the reflectivity curves. This behaviour is related to constructive and destructive interference phenomena which occur in the dielectric layer for both TE and TM modes. In fact, we create an energy modulation in reflection according to the angle of incidence. Lower is the index of refraction (ε_1), greater is the number of oscillations due to interferences in the rutile layer. In the case of the dielectric tensor (46), we can see that the Kerr rotation and the reflectivity (Figs. 8a and b) have the same variations of ones in (Figs. 6a and b) for the isotropic rutile of dielectric permittivity ε_1.

As we have seen in reference [13], the Kerr rotation reacts to the reflectivity fluctuations as a function of the angle of incidence. The Kerr effect gives minima of reflectivity when the reflectivity is high whereas it is maximum when the reflectivity is low in its variation of the angle of incidence (see Figs. 3b, 4b and 5b). We can notice that further minima and maxima occur in the Kerr rotation curve as a function of the angle of incidence if we compare those found in the reflectivity curves for increasing MgF_2 film thicknesses in both TE and TM modes. Moreover, we can notice that the Kerr rotation level stays approximatively constant for the several dielectric film thicknesses and for both modes of polarization, TE and TM (Figs. 3b, 4b and 5b). The minima observed in the Kerr rotation curves rather correspond to a vanishing Kerr effect in its variation as a function of the angle of incidence. Moreover, these cancellations of the Kerr effect increase as the MgF_2 film thickness becomes higher (Figs. 3b, 4b and 5b). So, we can notice that the addition of a dielectric film on a thin magneto-optical one tends to cancel the Kerr effect on several angles for greater MgF_2 film thicknesses. Moreover, these phenomena appear not only in the TM mode but also in the TE mode where a Kerr rotation modulation is created as a function of the angle of incidence. An important effect can be noticed: we can see that the minima of the Kerr rotation appear for the same angles in both TE and TM polarizations and for each MgF_2 film thicknesses, this confirms the presence of multiple reflections in the dielectric layer and this effect can be thus attributed to interference in the MgF_2 thin film. A cover by a dielectric layer therefore creates oscillations in the reflectivity and in the Kerr rotation as a function of the angle of incidence under the condition of total reflection, the same effect can also be brought to the fore in the specular reflection in the air.

3.2 Co/TiO_2 bilayer

As we have studied MgF_2, we are going to examine the reflectivity and also the Kerr rotation for a system composed by two layers Co/TiO_2 with a 10 nm film thickness of cobalt and a 450 nm of TiO_2 (the effective wavelength in TiO_2 is approximatively $\lambda_{\text{eff}}^{\text{TiO}_2} = 240$ nm, this film thickness corresponds to 2 $\lambda_{\text{eff}}^{\text{TiO}_2}$) (Fig. 1b).

According to the orientation of the TiO_2 principal axis, the reflectivity and the Kerr rotation have significant oscillations as a function of the angle of incidence. All the reflectivity curves show oscillations in both TE and TM modes (see Figs. 8a, 9a and 10a) as we have seen in the preceding section for MgF_2 which has an index of refraction lower than the rutile one ($n_{\text{MgF}_2} = 1.38$).

As a comparison, we calculated the reflectivity and the Kerr rotation relative to a Co/TiO_2 system where we consider the rutile as an isotropic material of dielectric permittivity ε_1 (Figs. 6a and b) and of dielectric permittivity ε_2 (Figs. 7a and b). We can thus conclude that, for the TM mode, the y-component is major compared to the z-component of the electric field reflected by the bilayer structure, the rutile anisotropy is thus more difficult to characterize in this case. In the case of the dielectric tensor (47), the reflectivity and also the Kerr rotation (Figs. 9a and b), in the TE mode, behave as the rutile is isotropic with a dielectric permittivity ε_1. Whereas for the TM mode, the reflectivity and the Kerr rotation have similar behaviors than Figure 7 where we consider rutile as an isotropic material of dielectric permittivity ε_2. In this case, we see effectively main differences in the reflectivity and in the Kerr effect compared to results discussed above for the orientation (46) (see Fig. 8). In the case of the dielectric tensor (48), the angular variation of the reflectivity and of the Kerr rotation (Figs. 10a and b) behave as the rutile is an isotropic material of dielectric permittivity ε_2 for the TE mode since this permittivity acts in the dielectric tensor on the x-component of the incident electric field. Whereas for the TM mode, the curves behave as if the rutile is an isotropic material of dielectric permittivity ε_1.

The comparison between the orientations (47) and (48) brings to the fore, as we have noticed before, the major aspect of the y-component of the electric field facing the z one for the TM mode.

We see thus that, in the case of a low permittivity, oscillations are more emphasized in the reflectivity and in the Kerr rotation as a function of the angle of incidence (Fig. 6) whereas these oscillations due to multiple reflections in the dielectric film tend to disappear when the dielectric permittivity is higher (Fig. 7) in the reflectivity and in the Kerr effect for the same rutile film thickness of 450 nm. The orientation of the crystal eigen axis plays an important role in the reflectivity and in the Kerr rotation curves as a function of the angle of incidence, consequently, this method can determine the ordinary

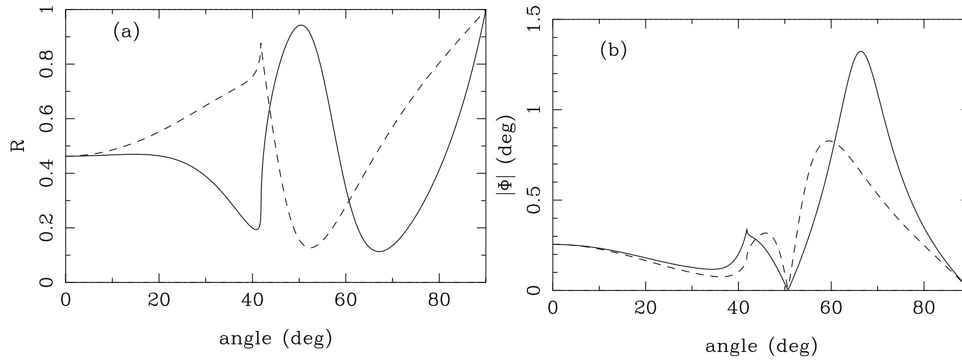

Fig. 6. For $\lambda = 0.633$ μm, reflectivity (a) and module $|\Phi|$ (b) of a bilayer composed of 10 nm of Co and of 450 nm of isotropic TiO_2 of dielectric permittivity $\varepsilon_1 = 6.67$ deposited on a glass substrate for the two modes: TE (dashed line) and TM (solid line) as a function of the angle of incidence.

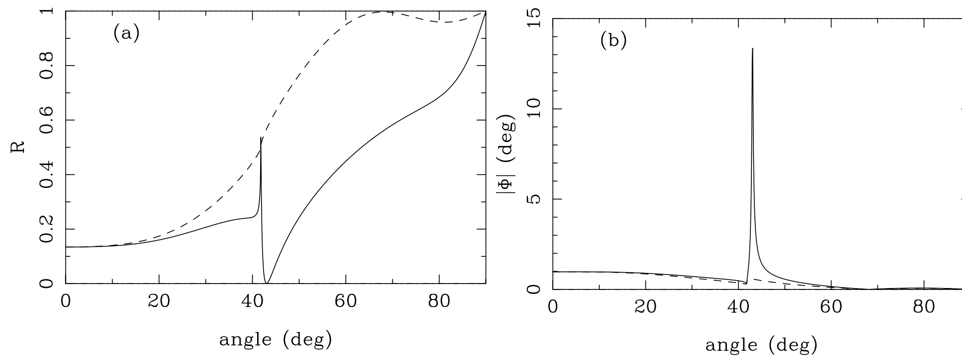

Fig. 7. For $\lambda = 0.633$ μm, reflectivity (a) and module $|\Phi|$ (b) of a bilayer composed of 10 nm of Co and of 450 nm of isotropic TiO_2 of dielectric permittivity $\varepsilon_1 = 8.24$ deposited on a glass substrate for the two modes: TE (dashed line) and TM (solid line) as a function of the angle of incidence.

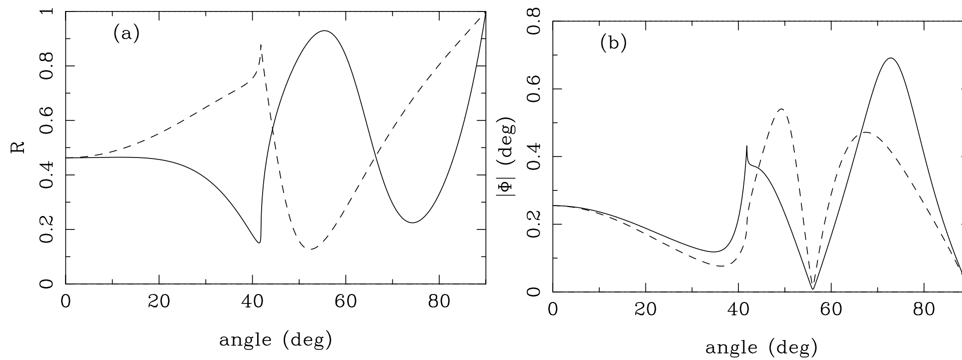

Fig. 8. For $\lambda = 0.633$ μm, reflectivity (a) and module $|\Phi|$ (b) of a bilayer composed of 10 nm of Co and of 450 nm of TiO_2 deposited on a glass substrate for the two modes: TE (dashed line) and TM (solid line) as a function of the angle of incidence for the orientation 46 of TiO_2.

and the extraordinary index of refraction for an anisotropic layer deposited on a substrate and the confirmation can be realized by the magneto-optical Kerr effect.

As we have noticed before, minima of Kerr rotation occur at the same angles for both TE and TM modes. We can see, as we have noticed before, that the Kerr effect vanishes simultaneously in TE and TM modes for the orientation (48) (Fig. 10), this effect is due to the interferences created by multiple reflections in the rutile dielectric layer.

For the same film thickness, an increase of index of refraction for a cover layer (MgF_2 and TiO_2) involves a decrease in the number of peaks relative to multiple reflections in the layer when analysing both reflectivity and Kerr rotation curves. For indices close to the substrate one, oscillations disturb the Kerr rotation curves and they are responsible for the cancellations of the Kerr effect for several angles of incidence according to the film thickness. This effect is of great interest for the determination of magnetization inside the magneto-optical Co layer because we can cancel the rotation of polarization phenomena which are optical properties of anisotropic materials and we could, thanks to these interferences, well-define the magnetization of the considered layer by an angular

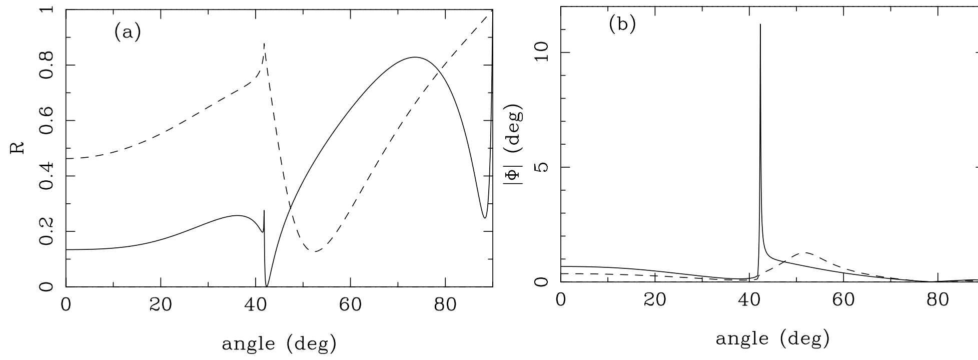

Fig. 9. For $\lambda = 0.633$ μm, reflectivity (a) and module $|\Phi|$ (b) of a bilayer composed of 10 nm of Co and of 450 nm of TiO_2 deposited on a glass substrate for the two modes: TE (dashed line) and TM (solid line) as a function of the angle of incidence for the orientation 47 of TiO_2.

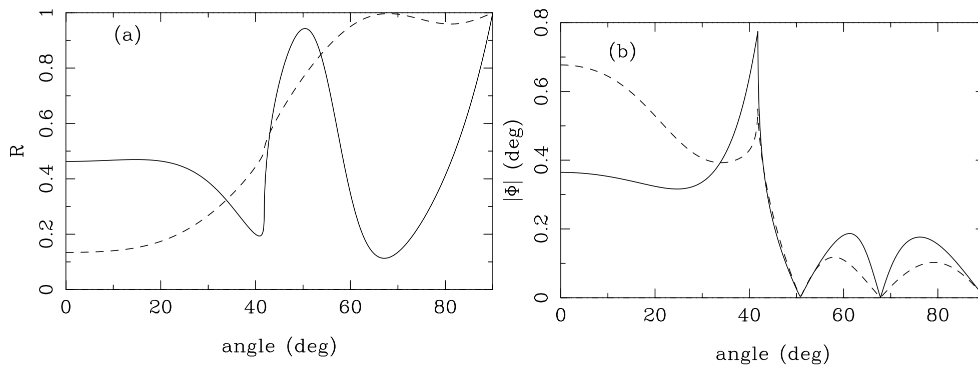

Fig. 10. For $\lambda = 0.633$ μm, reflectivity (a) and module $|\Phi|$ (b) of a bilayer composed of 10 nm of Co and of 450 nm of TiO_2 deposited on a glass substrate for the two modes: TE (dashed line) and TM (solid line) as a function of the angle of incidence for the orientation 48 of TiO_2.

study. The interferences are useful for the determination of a crystal eigen axis on account of the reflected energy curves and of the Kerr effect which changes due to the orientation of the principal axis of a given crystal compared to our coordinate system.

4 Dielectric/magnetic bilayers

4.1 Interferential modes in dielectric and isotropic thin films

In this second part, we want to show other resonance phenomena, those which occur in the components used for classical optics. We will show them in the context of magneto-optics. First, we will study the Perot-Fabry interferometer used in laser optics to calibrate wavelength spectra [20]. A Perot-Fabry interferometer is generally composed of a glass blade covered by a protective layer [21]. The system is illuminated in the air with an arbitrary angle of incidence and multiple reflections occur in the glass blade.

Here, we will study a similar system (see Fig. 1c) composed by a 2 μm dielectric MgF_2 film thickness (this one corresponds to 5 $\lambda_{\rm eff}^{\rm MgF_2}$) deposited on a glass substrate. We recovered the MgF_2 film by a 100 nm Co layer (see Fig. 1b). This Co thickness was chosen so as to saturate the cobalt layer reflectivity. This saturation is also necessary in order to eliminate, first, the virtual modes which drastically modify the interferential behaviours in the MgF_2 layer and second, the transmission by such a system.

Multiple reflections are produced in the MgF_2 layer and they create oscillations in the reflectivity curve as a function of the angle of incidence (see Fig. 11a). In the following curves (Figs. 11a and b), we calculate the reflectivity and also the Kerr rotation of this system as a function of the angle of incidence in the polar magnetization case. This study is interesting for the resonances of the system because interferential effects in the MgF_2 layer give an increase of the Kerr effect as we have noticed in the preceding section. Two principal effects are brought to the fore. First, oscillations occur in the reflectivity curve according to the angle of incidence for both TE and TM modes (Fig. 11a). Several interesting angles occur in these curves: one is similar to the Brewster angle corresponding to the cobalt layer for the MgF_2/Co interface and another "Brewster" one is attributed to the glass/MgF_2 interface. These angles appear in the reflectivity by the curves wrapping oscillations due to interferences produced in the MgF_2 layer for the TM mode. The critical glass/MgF_2 angle appears at 67 degrees. Beyond this angle, the wave is totally reflected and, consequently, the reflectivity is equal to unity. For the TE mode, we observe an increase of the reflectivity in which oscillations occur as a function of the angle of incidence until the glass/MgF_2

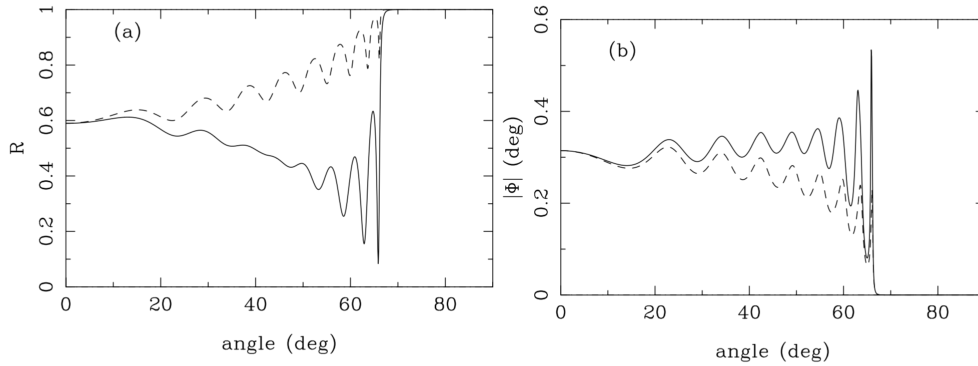

Fig. 11. For $\lambda = 633$ nm, (a) variation of the reflectivity as a function of the angle of incidence for both TM (solid line) and TE (dashed line) modes for the system of Figure 1 c (b) variation of $|\Phi|$ as a function of the angle of incidence for both TM (solid line) and TE (dashed line) modes.

critical angle beyond which the reflectivity is stabilised to one. Second, the Kerr rotation increases until angles similar to "Brewster's" beyond which it decreases according to the angle of incidence. Oscillations also occur in the Kerr effect and as the reflectivity decreases, the light wave goes through the cobalt layer and consequently, multiple reflections in this layer increase the Kerr rotation. Therefore, the Kerr effect is increasing in the MgF_2 film thickness and also in the glass substrate.

We do not have a vanishing Kerr effect in its variation as a function of the angle of incidence on the opposite of what we had in Section 3.1. This brings to the fore the comparison between a bilayer Co/MgF_2 and MgF_2/Co one thanks to the reflectivity and the Kerr rotation which do not have the same behaviours according to the angle of incidence. This also proves that the interferences can cancel the rotation of polarization effects (case of Co/MgF_2 bilayer) whereas they could give Kerr signals (case of MgF_2/Co bilayer). We can see that both bilayers involve interferences in the dielectric MgF_2 layer but they do not induce similar magneto-optical Kerr signals. Now, we will show another type of component which creates eigen modes in a system: the planar waveguides. These components (Perot-Fabry interferometer and waveguides) create eigen modes and thus, they are interesting in a magneto-optical point of view because they allow the increase of the Kerr effect.

4.2 Magneto-optical planar waveguides

As the magneto-optical Perot-Fabry interferometer, we will study the case of guided optics in planar geometry. Particularly, our study will show the effects on magneto-optical planar waveguides. A waveguide is generally composed of a guiding layer for which the index of refraction is n_2 deposited on a substrate (n_3) and they are in a medium of index of refraction n_1. In our case, the guiding layer will be rutile, the substrate is glass and they are in the air with two incident modes of polarization TE and TM. In order to have optical guiding in the layer (n_2), we must have $n_2 > n_3 \geq n_1$ which is our case. In the case of waveguides, for a given guiding layer thickness, the reflectivity

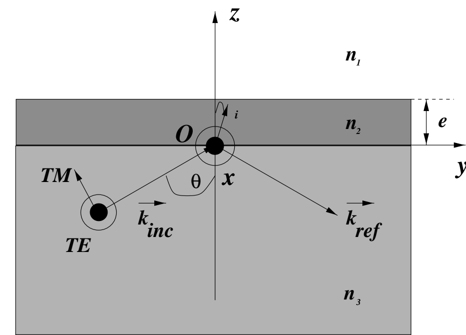

Fig. 12. Description of a planar waveguide in a general case. i is the angle of refraction in the layer of index n_2.

shows minima and maxima as a function of the angle of incidence, these minima correspond to pseudo-modes of propagation in the guiding layer which can modify the magneto-optical Kerr signals.

4.3 Definition of the modes in a planar waveguide

We call i_1 the angle beyond which there is total reflection on the rutile/air interface, it is defined by:

$$\sin i_1 = \frac{n_1}{n_2} \cdot$$

On the same way, we call i_2 the angle beyond which there is total reflection on the glass/rutile interface, it can be written as:

$$\sin i_2 = \frac{n_3}{n_2} \cdot$$

We call i the refracted angle in the rutile layer (see Fig. 12).

In a general case, three types of modes are defined. First, for $i < i_1$, classical interferences are produced in the rutile layer, this case is similar to the Perot-Fabry interferometer which was studied previously. Second, for $i_1 < i < i_2$, this is the case of substrate modes, a total reflection is produced on the rutile/air interface thus light beams are reflected in the layer and transmitted in the glass substrate. Finally, for $i > i_2$, these are

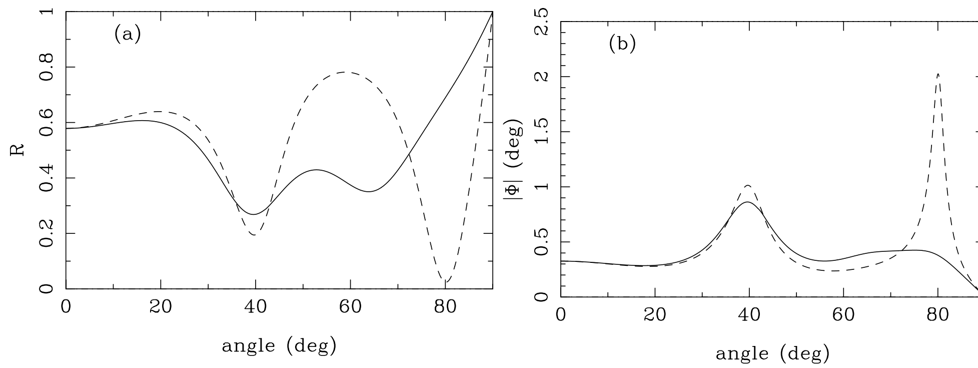

Fig. 13. For $\lambda = 633$ nm, variation of the reflectivity (a) and of the module $|\Phi|$ (b) as a function o f the angle of incidence for both TM (solid line) and TE (dashed line) for the system of Figure 1c and for an isotropic system $\varepsilon_1 = 6.67$.

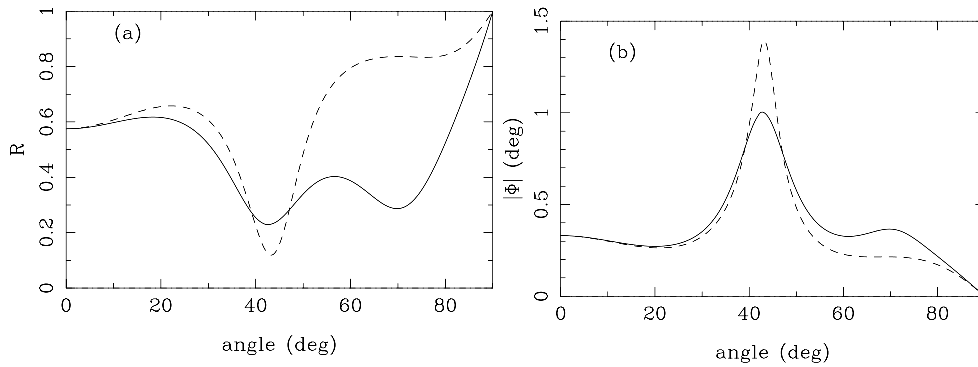

Fig. 14. For $\lambda = 633$ nm, variation of the reflectivity (a) and of the module $|\Phi|$ (b) as a function of the angle of incidence for both TM (solid line) and TE (dashed line) for the system of Figure 1c and for an isotropic system $\varepsilon_2 = 8.24$.

the guided modes, total reflection conditions are realized on the glass/rutile and also on the rutile/air interfaces which forbid a light beam to go out of the guiding layer, we must thus inject the light by the side of the guiding layer.

4.4 Magneto-optical rutile waveguide modes

We set a 1.1 μm rutile guiding layer (this thickness corresponds to 5 $\lambda_{\rm eff}^{\rm TiO_2}$) on a glass substrate covered by a 100 nm of Co in order to realize the condition of total reflection in the rutile/metal interface (see Fig. 1c). We observe substrate modes in the reflectivity curves as a function of the angle of incidence for $\lambda = 633$ nm. If we take the first orientation (46), we calculate the reflectivity and also the Kerr rotation as a function of the angle of incidence for both TE and TM incident modes (Fig. 15).

We illuminate the layers through the glass substrate with two modes: TE and TM associated with the laser beam. In this approach, the reflectivity shows minima and maxima as a function of the angle of incidence corresponding to the interferences in the rutile layer.

For the same reason (as the magneto-optical Perot-Fabry interferometer case), the 100 nm Co film thickness was chosen to saturate the metallic layer in order to eliminate effects due to the virtual modes and/or plasmon resonance of thin metallic film. This kind of resonances could modify the signals obtained in reflectivity and also in Kerr rotation for the planar waveguide.

In this approach, we want to bring to the fore not only magneto-optical effects due to the introduction of the cobalt layer but also the anisotropy effects due to the crystalline structure of rutile.

We want to observe how both reflectivity and Kerr rotation react when the principal axis of the crystal is rotating in our coordinate system ($Oxyz$). We have already defined the dielectric tensors for rutile (46), (47) and (48). As the Co/TiO_2 bilayer case, we calculated, as a reference, the reflectivity and the Kerr rotation of the system TiO_2/Co by supposing that the rutile is an isotropic material of dielectric permittivity $\varepsilon_1 = 6.67$ (Fig. 13) and of dielectric permittivity $\varepsilon_2 = 8.24$ (Fig. 14). We can notice that the reflectivity behave as the material is isotropic of dielectric permittivity ε_1 for both modes of polarization (Figs. 15a and 13a). In the TE mode, the reflectivity has the same behaviour as rutile is an isotropic medium of dielectric permittivity ε_1 because the x-component of the reflected electric field dominates the other ones. We can also notice that, according to the results in the TM mode, the y-component of the reflected electric field is greater than the z-component as we have noticed before in the case of the Co/TiO_2 bilayer in Section 3.2. The reflectivity shows minima, they correspond to the resonance modes of the system and particularly to the substrate modes described previously (Fig. 15a). The Kerr rotation reacts drastically when resonances occur in the system. Maxima for the Kerr rotation (Fig. 15b) correspond to the substrate modes which we found in the reflectivity curve as

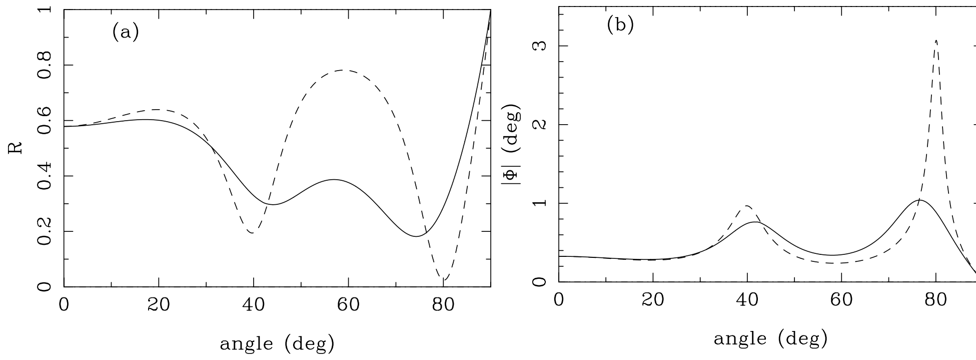

Fig. 15. For $\lambda = 633$ nm, (a) variation of the reflectivity as a function of the angle of incidence for both TM (solid line) and TE (dashed line) modes (b) variation of $|\Phi|$ as a function of the angle of incidence for both TM (solid line) and TE (dashed line) for the system of Figure 1c for an anisotropic system with the dielectric tensor (46).

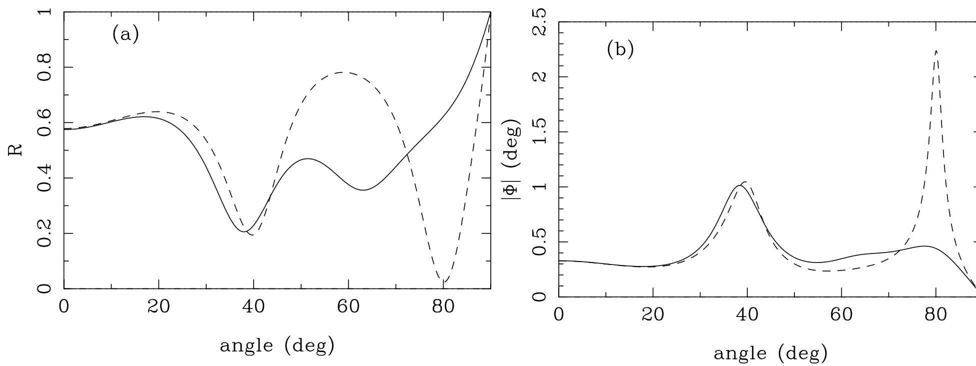

Fig. 16. For $\lambda = 633$ nm, (a) variation of the reflectivity as a function of the angle of incidence for both TM (solid line) and TE (dashed line) modes (b) variation of $|\Phi|$ as a function of the angle of incidence for both TM (solid line) and TE (dashed line) for the system of Figure 1c for an anisotropic system with the dielectric tensor (47).

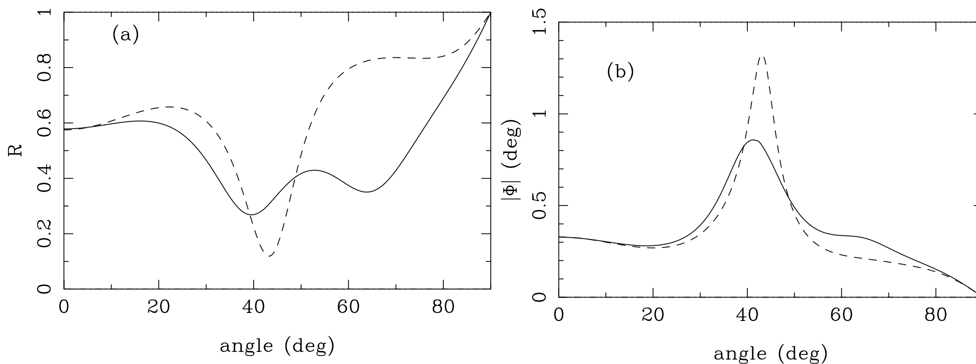

Fig. 17. For $\lambda = 633$ nm, (a) variation of the reflectivity as a function of the angle of incidence for both TM (solid line) and TE (dashed line) modes (b) variation of $|\Phi|$ as a function of the angle of incidence for both TM (solid line) and TE (dashed line) for the system of Figure 1c for an anisotropic system with the dielectric tensor (48).

a function of the angle of incidence (see Fig. 15a). This increase of the Kerr effect around the eigen modes of the system is consistent with results obtained previously in the Co/Au systems in [13] and also with the magneto-optical Perot-Fabry interferometer of the preceding section. If we take the case of the second orientation (47) of the eigen axis for the rutile, we can notice that for the TE mode, the reflectivity behaves as the rutile is an isotropic medium of dielectric permittivity ε_1 whereas for the TM mode, it reacts as an isotropic material of dielectric permittivity ε_2 (Fig. 16a) This confirms that the parallel components of the reflected electric field are greater than the perpendicular one. This effect was already seen in the case of a Co/TiO_2 bilayer. In the TM mode, the number of minima is not the same in the reflectivity curve as a function of the angle of incidence compared to the preceding orientation (46) (see Figs. 15a and 16a). Thus, the optical orientation of the crystal determines the reflectivity according

to the incident polarization mode which we chose. The Kerr rotation still increases around the resonance modes of the system (Fig. 16b). The number of minima in the reflectivity and also the number of maxima in the Kerr rotation, when using different orientations of the principal axis, show a modification in the crystallographic orientation of the rutile layer in the TM mode. This situation is experimentally significant because we can determine accurately the crystallographic anisotropy of a dielectric film. In the case of the third dielectric tensor for the rutile (48), we notice that in the TE mode, the reflectivity varies as the system is an isotropic medium of dielectric permittivity ε_2 whereas for the TM mode, it behaves as an isotropic material of dielectric permittivity ε_1 as a function of the angle of incidence (Fig. 17a). Maxima of Kerr rotation correspond to the several substrate modes for this waveguide (Fig. 17b). As we have noticed in the preceding section, the Kerr effect does not vanish for different angles whereas this behavior was observed for the Co/TiO_2 bilayer.

5 Conclusion

Two crucial points are brought to the fore in this paper. First, the Kerr rotation drastically reacts for all resonance phenomena in the system by several peaks corresponding to reflectivity minima. Using the components of classical optics (*i.e.* the interferences, the substrate modes and also the plasmon resonance in a metal case), the Kerr effect increases around the resonances. This effect, which was purely energetical, can be experimentally observable by the rotation of polarization in reflection according to the incident polarization. The increase of the Kerr rotation and the reflected energy can be measured around the resonances in the far-field. It shows an experimental facility for the setups. Second, we separate two types of anisotropy: the anisotropy effects induced by the crystalline structure (such as an uniaxial crystal (rutile)) and the Kerr rotation which is an anisotropic effect induced by applying an external magnetic field. This classical approach of calculation, for the reflected energy and for the Kerr rotation, described accurately the crystal orientation compared to the coordinate system of the surface. This study can be extended to biaxial crystals. Thanks to this procedure, we realise a characterisation method of thin films in an optical way. This method is valid if the deposition of the thin film keeps the direction of the eigen axis for crystal monolayers deposited on a glass substrate.

Professor O. Marti and the members of Abteilung Experimentelle Physik are acknowledged.

References

1. M. Hayashi, T. Katayama, J. Magn. Magn. Mater. **126**, 547 (1993).
2. M.E. Brubaker, E.R. Moog, C.H. Sowers, J. Zak, S.D. Bader, J. Magn. Magn. Mater. **103**, L7 (1992).
3. J. Zak, E.R. Moog, C. Liu, S.D. Bader, J. Magn. Magn. Mater. **89**, 107 (1990).
4. T.W. McDaniel, R.H. Victora, in *Handbook of magneto-optical data recording: materials, subsystems, techniques*, edited by T.W. McDaniel, R.H. Victora (Noyes Publications, 369 Fairview Avenue, Westwood, New Jersey, 1997).
5. C.W. Lee, K.H. Rim, Y.W. Kim, Jpn. J. Appl. Phys. **32**, 5443 (1993).
6. S. Tamada, S. Igarashi, S. Sakamoto, H. Nakayama, M. Yoshida, Y. Nakane, JAP **28**, 67 (1989).
7. M. Kaneko, J. Magn. Magn. Mater. **148**, 351 (1995).
8. R. Atkinson, J. Magn. Magn. Mater. **124**, 333 (1993).
9. V.I. Safarov, V.A. Kosobukin, C. Hermann, G. Lampel, J. Peretti, Phys. Rev. Lett. **73**, 3584 (1994).
10. A. Otto, Z. Phys. **216**, 398 (1968).
11. H. Raether, *Surface plasmons on Smooth and Rough Surfaces and on Gratings* (Springer, Berlin, 1988).
12. Y. Levy, M. Jurich, J.D. Swalen, J. Appl. Phys. **57**, 2601 (1985).
13. N. Richard, A. Dereux, T. David, E. Bourillot, J. P. Goudonnet, F. Scheurer, E. Beaurepaire, G. Garreau, Phys. Rev. B **59**, 5936 (1999).
14. C. Girard, A. Dereux, Rep. Prog. Phys. **59**, 657 (1996).
15. A.A. Maradudin, D.L. Mills, Phys. Rev. B **11**, 1392 (1975).
16. A. Yaghjian, Proceedings of the IEEE **68**, 248 (1980).
17. E.D. Palik, in *Handbook of optical constants of solids*, edited by E.D. Palik (Academic Press, New York, 1991).
18. G.S. Krinchik, V.A. Artem'ev, Sov. Phys. JETP **26**, 1080 (1968).
19. A. Yariv, P. Yeh, in *Optical waves in crystals*, edited by J.W.S. Inc. (Wiley, 1984).
20. J.M. Aguirregabiria, L. Bel, Phys. Rev. A **36**, 3768 (1987).
21. F. Lemarquis, E. Pelletier, Appl. Opt. **35**, 4987 (1996).